Guided Ion Beam and Theoretical Study of the Reactions of Ir^+ with H_2, D_2, and HD†

Feng-Xia Li, Xiao-Guang Zhang, and P. B. Armentrout*

Chemistry Department, University of Utah, 315 S. 1400 E. Rm 2020, Salt Lake City, Utah 84112

Received: June 3, 2004; In Final Form: October 20, 2004

We present the kinetic energy dependence of reactions of the late third-row transition metal cation Ir^+ with H_2, D_2, and HD measured using a guided ion beam tandem mass spectrometer. A flow tube ion source produces Ir^+ ions in its electronic ground state term and primarily in the ground spin−orbit level. Corresponding state-specific reaction cross sections are obtained. The kinetic energy dependence of the cross sections for forming IrH^+ and IrD^+ are analyzed to give a 0 K bond dissociation energy of $D_0(Ir^+-H) = 3.12 \pm 0.06$ eV. Ab initio calculations at the B3LYP/HW+/6-311+G(3p), BHLYP/HW+/6-311+G(3p), and QCISD(T)/HW+/6-311+G(3p) levels performed here show reasonable agreement with the experimental bond energies and with the previous theoretical values available. Theory also provides the electronic structures of these species and the reactive potential energy surfaces. We also compare this third-row transition metal system with those of the first-row and second-row congeners Co^+ and Rh^+. We find that Ir^+ has a stronger M^+-H bond, which can be explained by the lanthanide contraction and relativistic effects that alter the relative size of the valence s and d orbitals. Results from reactions with HD provide insight into the reaction mechanisms and indicate that Ir^+ reacts largely via an insertion mechanism, in contrast with the lighter group 9 metal ions Co^+ and Rh^+ which react via direct mechanisms.

Introduction

Iridium complexes are good homogeneous C−H bond activation catalysts in solution[1] and react by an oxidative addition mechanism at an unsaturated Ir center. To develop more efficient and economical homogeneous catalysts, we need to understand the various factors that contribute to the reactivity of interest. For this purpose, gas-phase studies are a good starting point for providing information on the intrinsic properties of metals in the absence of solvent and stabilizing ligands and also form an ideal interface for theoretical calculations on such complex elements.

The largely covalent M^+-H bonds have been studied with increasing accuracy for the first-row and second-row transition metals as a result of developments both in experiments and theoretical calculations.[2−15] Among the experimental techniques available for measuring the thermodynamics of gas-phase species, guided ion beam methods can examine reactions at hyperthermal energies, and thereby have the ability to study endothermic reactions. This permits the determination of the bond dissociation energies (BDEs) for M^+-H from an analysis of the kinetic energy dependence of reaction 1 and its isotopic analogues.

$$M^+ + H_2 \rightarrow MH^+ + H \qquad (1)$$

Such ion beam studies also provide insight into the electronic requirements for the activation of dihydrogen by transition metal ions and periodic trends in the reactivity of these metal ions. Previously, we have applied this methodology to all of the first-row and second-row transition metals except Tc.[5,8,10−14,16−20]

Experimental studies are less extensive for the third-row transition metal cations, although there are a number of studies in the literature.[21−32] Theoretical studies of metal dihydrides include all of the third-row transition metal cations.[33−41] An ongoing project in our laboratory is to systematically study the activation of dihydrogen by the third-row transition metal cations and determine the M^+-H BDEs by using guided ion beam tandem mass spectrometry. These studies allow us to compare the bond energies and other characteristics of all transition metal hydrides, thereby establishing periodic trends. Of particular interest in the third row is the study of the influence of strong spin−orbit coupling on the reactivity. Recent studies in our laboratories have examined reactions of dihydrogen with Ta^+, W^+, Re^+, and Pt^+.[42−44] In the present work, we extend our studies to include Ir^+.

Using a Fourier transform ion cyclotron resonance (FTICR) spectrometer, Irikura and Beauchamp found that the dehydrogenation of CH_4 at thermal energies by Ir^+ is 70% efficient, among the most efficient of all the transition metal cations for this process.[22] However, there is still little thermochemical information for these reactions. Here, we study the simple reaction 1, the activation of a covalent single bond, analogous to the activation of the C−H and C−C bonds of interest in catalytic processes. We report the absolute cross sections as a function of kinetic energy for reactions of dihydrogen with Ir^+, and the bond dissociation energy (BDE) for IrH^+ is determined. Such small systems allow detailed theoretical calculations that can be compared with the experimental results. Thus, theoretical calculations on the IrH^+ and IrH_2^+ species are also performed to assign electronic structures and explore the potential energy surfaces for reaction. These are compared to the previous results of Ohanessian et al.[33] for IrH^+ and Balasubramanian and co-workers for IrH^+ and IrH_2^+.[34,41] To get information about the reaction mechanisms, we also investigate the reactions of Ir^+ with HD over a wide range of kinetic energies. Such reactions with HD have been shown to provide useful mechanistic information.[8,10,12−14,16,17]

† Part of the special issue "George W. Flynn Festschrift".

10.1021/jp047597f CCC: $30.25
Published on Web 01/20/2005

Experimental Section

General Procedures. Cross sections for reactions of Ir^+ with H_2, D_2, and HD are measured using a guided ion beam tandem mass spectrometer that has been described in detail previously.[45] Atomic Ir^+ metal ions are generated in the direct current discharge flow tube source described below.[46] The ions are extracted from the source, accelerated, and focused into a magnetic sector momentum analyzer for mass selection of primary ions. Mass-selected ions are decelerated to a desired kinetic energy and focused into an octopole ion beam guide, which uses radio frequency electric fields to trap the ions in the radial direction and ensure complete collection of reactant and product ions.[47,48] The octopole passes through a static gas cell that contains the reaction partner at a low pressure (usually $\leq$0.3 mTorr) so that multiple ion−molecule collisions are improbable. All products reported here result from single bimolecular encounters, as verified by pressure dependence studies. Product and unreacted Ir^+ ions drift to the end of the octopole where they are extracted, focused, and passed through a quadrupole mass filter for mass analysis of the products and subsequently detected with a secondary electron scintillation ion detector using standard pulse counting techniques. Ion intensities are converted to absolute cross sections after correcting for background signals.[49] Absolute uncertainties in cross section magnitudes are estimated to be ±20%.

The kinetic energy dependence of the ions is varied in the laboratory frame by scanning the direct current (dc) bias on the octopole with respect to the potential of the ion source region. Ion kinetic energies in the laboratory frame, E_{lab}, are converted to energies in the center-of-mass frame, E_{cm}, using the formula $E_{cm} = E_{lab}m/(m + M)$, where m and M are the neutral and ionic reactant masses, respectively. All energies reported below are in the center-of-mass frame unless otherwise noted. Two effects broaden the cross section data: the thermal motion of the neutral reactant gas (Doppler broadening) and the kinetic energy distribution of the reactant ion.[50,51] The absolute zero and distribution of the ion kinetic energies are determined using the octopole beam guide as a retarding potential analyzer as described previously.[49] The distribution of ion kinetic energies is nearly Gaussian and has a typical full width at half-maximum (fwhm) between 1 and 1.7 eV (lab) in these studies. The uncertainties in the absolute energy scale are ±0.05 eV (lab).

Ion Source. Atomic Ir^+ metal ions are formed in a direct current discharge flow tube (DC/FT) source.[46] This source consists of a cathode held at a high negative voltage (0.7−1.5 kV) over which a flow of approximately 90% He and 10% Ar passes at a total pressure of 0.3−0.5 Torr and ambient temperature. The cathode in this work is iridium foil attached to an iron holder. Ar^+ ions created in the discharge are accelerated toward the metal cathode, thereby sputtering Ir^+ ions. These ions are then swept down a 1 m long flow tube. The flow conditions used in this ion source provide about 10^5 thermalizing collisions between an ion and He (about 10^4 collisions with Ar) before the ions enter the guided ion beam apparatus. Generally, these conditions have been found to thermalize the ions, thereby producing atomic ions in their ground electronic state. For example, on the basis of comparisons to a surface ionization source, the DC/FT source was found to generate Sc^+,[52] Fe^+,[53] Co^+,[54] Ni^+,[55] Ru^+,[13] Rh^+,[13] and Pd^+ [13] ions with an average electronic temperature of 700 ± 400 K and Y^+, Zr^+, Nb^+, and Mo^+ ions with an average electronic temperature of 300 ± 100 K.[14] The populations of Ir^+ ions created under such conditions are listed in Table 1, where the energies are taken from the spectroscopic work of Kleef and Metsch.[56] Clearly, most Ir^+ ions are in the ground electronic state, a^5F_5 ($5d^76s^1$), even at the highest likely temperature. From the populations of ions at 700 ± 400 K, the average electronic energy is calculated to be 0.002 + 0.013/−0.002 eV for Ir^+.

TABLE 1: Electronic States of Iridium Cations

term	J	electron configuration	energy[b] (eV)	population[a] (%) 300 K	700 K	1100 K
^5F	5	$5d^76s^1$	0.000	100.00	99.15	95.08
^3F	4	$5d^8$	0.281	0.0	0.77	4.01
^3P	2	$5d^8$	0.383	0.0	0.08	0.76
^5F	4	$5d^76s^1$	0.594	0.0	0.0	0.15
^5F	3	$5d^76s^1$	1.015	0.0	0.0	0.0

[a] Maxwell−Boltzmann distribution at the indicated temperature. [b] Reference 56.

Data Analysis. The kinetic energy dependence of product cross sections is analyzed to determine E_0, the energy threshold for product formation at 0 K. E_0 differs from the apparent threshold observed under laboratory conditions because of the Maxwell−Boltzmann velocity distribution and internal energy of the neutral reactants, and the kinetic and internal energy distributions of the reactant ions. Each of these contributions allows reactions to occur at energies below E_0. To determine E_0, endothermic reaction cross sections are modeled using eq 2[18−20,57−61]

$$\sigma(E) = \sigma_0[\Sigma g_i(E + E_{el} + E_i - E_0)^n/E] \times [1 - P_D] \quad (2)$$

where σ_0 is an energy-independent scaling factor, E is the relative kinetic energy of the reactants, E_{el} is the electronic energy of the metal cation, and n is an adjustable parameter. P_D is the dissociation probability, which relies in a complicated way detailed elsewhere[61] on two parameters: E_D, the onset for product dissociation, and p, a parameter similar to n. There is an explicit sum of contributions from rovibrational states of reactants at 300 K, denoted by i, having energies E_i and populations g_i, where $\sum g_i = 1$. The various sets of vibrational frequencies and rotational constants used to determine E_i in this work are taken from the literature for H_2, D_2, and HD.[62] The average internal energy for H_2 and D_2 is 0.026 eV. As noted above, E_{el} at 700 ± 400 K is believed to be 0.002 + 0.013/−0.002 eV for Ir^+. Before comparison with the experimental data, eq 2 is convoluted with the kinetic energy distributions of the ions and neutral reactants at 300 K. The σ_0, n, and E_0 parameters are then optimized using a nonlinear least-squares analysis to give the best reproduction of the data.[59] Error limits for E_0 are calculated from the range of threshold values for different data sets over a range of acceptable n values combined with the absolute uncertainty in the energy scale.

Theoretical Calculations

All quantum chemistry calculations reported here are computed using the B3LYP hybrid density functional method,[63,64] except as noted, and performed with the GAUSSIAN 98 suite of programs.[65] In all cases, the thermochemistry reported here is corrected for zero point energy effects. The 6-311+G(3p) basis set is used for hydrogen. This method and basis set gives deviations from experiment of <0.03 eV for the bond energy of H−H (4.505 eV calculated versus 4.478 eV experimental).[62] The 60 core electrons of iridium are described by the relativistic effective core potential (ECP) of Hay and Wadt (HW),[66] with valence electrons described by the Los Alamos double-ζ (LANL2DZ) basis set. The basis set is optimized for neutral atoms, whereas the positive charge differentially contracts the

s orbitals compared to the d orbitals. Hence, all calculations were performed with an altered HW-ECP basis for Ir^+ as described by Ohanessian et al. (HW+).[33]

Holthausen et al.[67] carefully considered the most appropriate choice for a level of theory for the first- and third-row transition metal methyl cations, species analogous to the metal hydride cations considered here because both have single covalent metal−ligand bonds. These authors used B3LYP, Becke-Half-and-Half-LYP (BHLYP), and QCISD(T) methods with a basis set consisting of a polarized double-ζ on C and H and the Hay−Wadt relativistic ECP with valence electrons added. The symmetries of the metal methyl species were constrained to C_{3v}. Upon comparison with experimental results for the first-row MCH_3^+ species (M = Sc−Cu),[18,19] these authors conclude that the B3LYP functional overbinds, whereas the BHLYP functional and the QCISD(T) methods perform more accurately. Mean absolute deviations from experiment were 0.41, 0.18, and 0.20 eV, respectively. Likewise, the bond energies calculated using B3LYP were higher than those for BHLYP and QCISD(T) for the third-row metal methyl cations. Given these results, we also performed calculations for the IrH^+ species using the BHLYP functional and QCISD(T) methods, where the latter utilizes geometries calculated at the BHLYP/HW+/6-311+G(3p) level, as these give lower energies than B3LYP geometries. Such calculations will be explicitly noted, and unless otherwise designated, our results will refer to a B3LYP/HW+/6-311+G-(3p) level of theory. For IrH_2^+ species where multiple bonds to Ir^+ are formed, only the B3LYP functional is used. This choice is rationalized on the basis of the results of Holthausen, Mohr, and Koch[68] for metal−methylene cations and our own studies of MCH_x^+ ($x = 0-2$) species.[25,44]

The experimental BDE refers to the ground spin−orbit state at 0.0 eV, a^5F_5 for Ir^+.[56] In contrast, calculations are referenced to the statistically weighted mean of all spin−orbit levels in the ground state term, 0.642 eV for Ir^+ (a^5F).[56] Because our calculations do not explicitly include spin−orbit interactions, it is possible that calculated bond energies should be corrected by this different asymptotic energy before comparison with experimental values. However, Balasubramanian and co-workers have found that the spin−orbit effects for IrH^+ and IrH_2^+ are also large.[34,41] For instance, their calculations indicate spin−orbit effects can be as large as 1.36 eV for IrH^+ but are generally smaller for most states. Because spin−orbit effects influence the energetics of reactants, intermediates, and products in reaction 1, we do not apply corrections in the present work, as the magnitude of the effects are unknown for IrH^+ and IrH_2^+. This implicitly assumes that the spin−orbit corrections largely cancel.

Experimental and Theoretical Results

Reactions with H_2 and D_2. Figure 1 shows cross sections as a function of kinetic energy for the bimolecular reaction of H_2 with Ir^+ produced in the DC/FT source. A single product ion, as shown in reaction 1, is observed. Comparable results for reaction with D_2, reaction 3, are shown in Figure 2.

$$Ir^+ + D_2 \rightarrow IrD^+ + D \quad (3)$$

The magnitudes of the $Ir^+ + H_2$ and $Ir^+ + D_2$ reaction cross sections are very similar. The cross sections rise from apparent thresholds near 1 eV and reach maxima near the dissociation energy of H_2, 4.478 eV, or D_2, 4.556 eV.[62] Above this energy, IrH^+ (IrD^+) may be formed with an internal energy in excess of its bond dissociation energy. Therefore, the IrH^+ (IrD^+) product begins to dissociate in the overall reaction 4

$$Ir^+ + H_2\,(D_2) \rightarrow IrH^+\,(IrD^+) + H\,(D) \rightarrow Ir^+ + 2H\,(D) \quad (4)$$

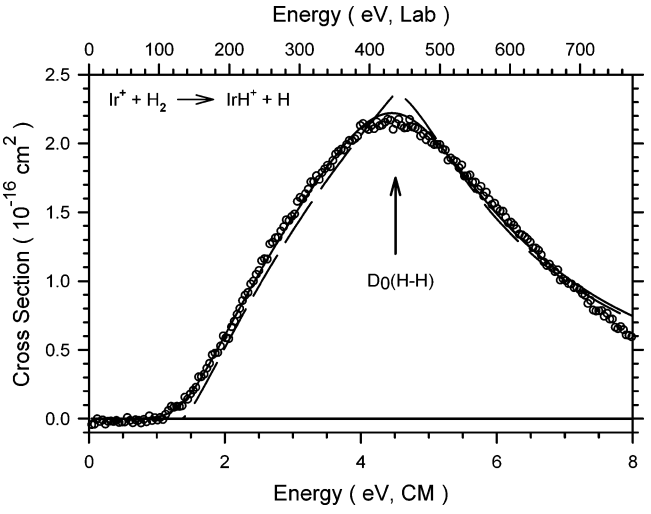

Figure 1. Cross sections for reaction of Ir^+ (^5F) with H_2 as a function of kinetic energy in the center-of-mass frame (lower axis) and the laboratory frame (upper axis). The model of eq 2 with parameters from Table 2 is shown as a dashed line. The solid line shows this model convoluted over the kinetic and internal energy distributions of the reactant neutral and ion. The arrow indicates D_0(H−H) at 4.478 eV.

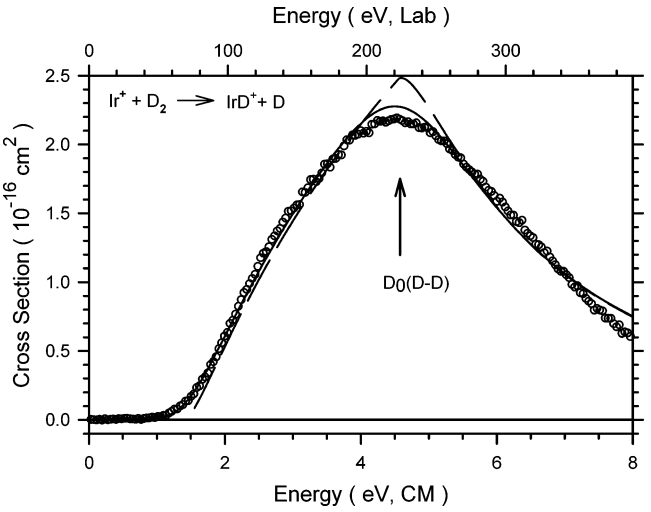

Figure 2. Cross sections for reaction of Ir^+ (^5F) with D_2 as a function of kinetic energy in the center-of-mass frame (lower axis) and the laboratory frame (upper axis). The model of eq 2 with parameters from Table 2 is shown as a dashed line. The solid line shows this model convoluted over the kinetic and internal energy distributions of the reactant neutral and ion. The arrows indicate D_0(D−D) at 4.556 eV.

Reactions with HD. Ir^+ reacts with HD to yield reactions 5 and 6, as shown in Figure 3.

$$Ir^+ + HD \rightarrow IrH^+ + D \quad (5)$$

$$\rightarrow IrD^+ + H \quad (6)$$

Because of the close proximity of the product masses, there can easily be some overlap between these signals depending on the mass resolution used in the quadrupole mass filter. For this experiment, high-resolution conditions can be used to separate these products without sacrificing efficient collection of the product ions. The accuracy of the final results is confirmed

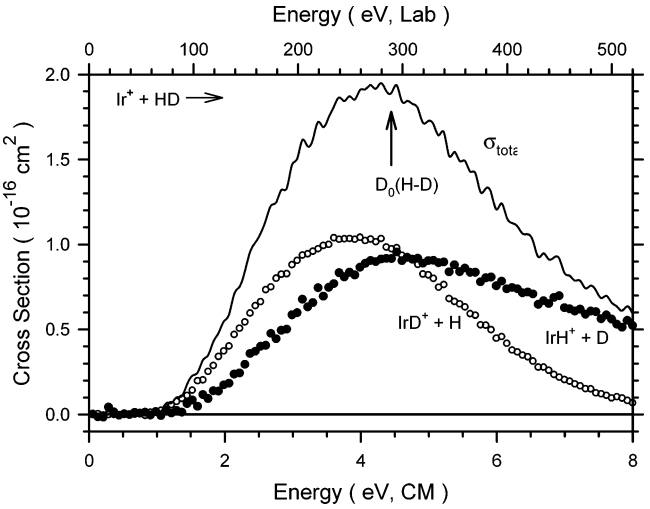

Figure 3. Cross sections for reaction of Ir^+ (^5F) with HD as a function of kinetic energy in the center-of-mass frame (lower axis) and the laboratory frame (upper axis). The arrow indicates D_0(H−D) at 4.514 eV.

TABLE 2: Parameters of eq 2 Used in Modeling Reactions 1 and 3 and the Resultant Bond Energies

reaction	σ_0	n	E_0 (eV)	$D_0(Ir^+-H)$ (eV)
$Ir^+ + H_2$	2.1 ± 0.1	1.5 ± 0.1	1.35 ± 0.04	3.13 ± 0.04
$Ir^+ + D_2$	2.3 ± 0.2	1.4 ± 0.1	1.42 ± 0.04	3.10 ± 0.04^a

[a] Value corrected for a zero point energy difference of 0.041 eV. See text.

by good agreement between the magnitudes of the total cross sections for the HD system and those of the H_2 and D_2 systems (Figures 1 and 2).

The total cross section in the HD system exhibits endothermic behavior and rises from a threshold that is similar to those of the H_2 and D_2 systems. The total cross section reaches a maximum near the bond dissociation energy of HD, 4.514 eV.[62] The individual IrH^+ and IrD^+ cross sections behave somewhat differently with energy such that the IrD^+ cross section rises more rapidly from a slightly earlier apparent onset than the IrH^+ cross section. This is because the $IrD^+ + H$ product channel has a lower energy threshold by a zero point energy difference of 0.041 eV (see below). At higher energies, the IrD^+ cross section declines at an energy somewhat before the onset of dissociation because of competition with the $IrH^+ + D$ channel, such that the IrH^+ channel dominates at higher energies. This observation shows that the IrH^+ product ion is stabilized by removal of energy by the D atom product relative to $IrD^+ + H$. The relative high-energy behavior shows that the heavier D atom carries away more energy from IrH^+ than the H atom carries away from IrD^+. This effect is typical of atomic ion reactions with HD[10,13,14,17] and has been discussed in detail elsewhere.[17,69−71]

Thermochemistry. The endothermic cross sections from the H_2 and D_2 reaction systems are analyzed in detail using eq 2, which accounts for dissociation at energies above the onset of reaction 4. At these high energies, E_D is fixed to the H_2 (D_2) bond energy and the optimum value of p is found to be 2. Typical models of the data from threshold to ~7 eV are shown in Figures 1 and 2 and reproduce the experimental results very well.

The optimum values of the parameters in eq 2 are listed for these systems in Table 2. These values represent average parameters for nine data sets for each system. Because of the appreciable kinetic energy distribution of the light H_2 and D_2 reactants, the thresholds listed differ appreciably from the apparent thresholds for these reactions, as shown in Figures 1 and 2. Because the rotational, vibrational, translational, and electronic energy distributions of reactants are explicitly included in the modeling, the E_0 threshold energies determined using eq 2 correspond to 0 K values. The BDEs for the metal−ligand cations observed in reactions 1 and 3 can be calculated using eq 7

$$D_0(Ir^+-L) = D_0(L-L) - E_0 \qquad (7)$$

where D_0(H−H) = 4.478 eV and D_0(D−D) = 4.556 eV.[62] This equation assumes that there is no activation barrier in excess of the endothermicity of the reaction, an assumption that is often true for ion−molecule reactions because of the long-range attractive forces.[59] This assumption is also consistent with the calculated potential energy surfaces discussed below.

Table 2 provides a summary of the Ir^+−H bond energies derived from the present experiments with both H_2 and D_2. For the D_2 result, this requires correcting for the zero point energy differences between $D_0(IrD^+)$ and $D_0(IrH^+)$. This correction uses a vibrational frequency of 2273 cm^{-1} for IrH^+ and 1612 cm^{-1} for IrD^+, as determined in the present calculations. Thus, the zero point energy difference is 0.041 ± 0.004 eV, assuming a 10% uncertainty in the frequency. (Use of a 2372 cm^{-1} frequency for IrH^+ determined by Ohanessian et al.[33] yields a difference of 0.043 eV, which does not change the final result.) Note that the Ir^+−H bond energies obtained from the H_2 and D_2 systems are in good agreement with one another (Table 2). We take the weighted average of these two values as our final experimental result of 3.12 ± 0.06 eV, where the uncertainty is two standard deviations of the mean.

IrH^+ Electronic Structure. GVB calculations indicate that IrH^+ has a $^4\Sigma^-$ ground state with a covalent bond formed between a singly occupied sd hybridized (37% 6s and 63% 5d) orbital on Ir^+ (a^5F) and the singly occupied 1s orbital on H.[33] Such hybridization is particularly efficient in the third-row transition metals because the lanthanide contraction and relativistic effects make the 6s orbital comparable in size and energy to the 5d orbitals. The GVB calculations also indicate that there is a low-lying $^4\Phi$ state, calculated to lie only 0.16 eV above the $^4\Sigma^-$ state.[33] They suggested that spin−orbit coupling could alter the order of these states such that the $^4\Phi$ state probably becomes the ground state. GVB theory followed by correlation consistent configuration interaction (CCCI) calculations[33] provides a BDE for IrH^+ of 2.85 eV for the $^4\Sigma^-$ state, somewhat lower than the experimental result of 3.12 ± 0.06 eV. They also got a BDE of 2.69 eV for the $^4\Phi$ state. Dai, Huang, and Balasubramanian (DHB)[41] also calculated spectroscopic constants and potential energy curves for IrH^+ using the complete active space multiconfiguration self-consistent field (CAS-MCSCF) followed by first-order configuration interaction (FOCI) and multireference singles + doubles (MRSDCI). They found the ground state of IrH^+ is $^4\Sigma^-$ in the absence of spin−orbit interaction. They also identified a low-lying $^4\Phi$ state, which lies only 0.19 eV (FOCI) and 0.20 eV (MRSDCI) above the $^4\Sigma^-$ ground state. They determined $D_e(Ir^+-H)$ values of 2.85 eV (FOCI) and 3.28 eV (MRSDCI) for the $^4\Sigma^-$ ground state. After correcting for a zero point energy of 0.14 eV for IrH^+ (from our calculation for the $^4\Sigma^-$ ground state), this gives 0 K BDEs of 2.71 eV (FOCI) and 3.14 eV (MRSDCI) for the $^4\Sigma^-$ ground state. The latter value is in good agreement with our experimental value of 3.12 ± 0.06 eV.

Our calculations also find a $^4\Sigma^-$ ground state with the $^4\Phi$ state lying another 0.27 eV higher (Table 3). The 0 K bond

TABLE 3: Theoretical Geometries and Energies for IrH^+ [a]

state	r_e(Ir−H) (Å)	E_{rel} [b] (eV)	frequency (cm^{-1})
$^4\Sigma^-$	1.570	0	2273
$^4\Phi$	1.583	0.269	2246
$^2\Delta$	1.558	0.458	2328
$^2\Pi$	1.573	0.702	2302
$^2\Phi$	1.584	0.842	2250
$^2\Pi$	1.583	0.981	2232
$^2\Sigma^-$	1.621	1.528	2096
$^4\Pi$	1.849	4.427	937
$^4\Delta$	3.255	4.548	199

[a] Results of B3LYP/HW+/6-311+G(3p) calculations. [b] Energies relative to the ground state including zero point energies.

energy for the $^4\Sigma^-$ ground state from our calculation is 3.25 eV, close to the experimental value 3.12 ± 0.06 eV (Table 2). Bond lengths for the $^4\Sigma^-$ and $^4\Phi$ states are 1.570 and 1.583 Å, which are in excellent agreement with those from Ohanessian et al., 1.560 and 1.583 Å, respectively,[33] and from DHB, 1.567 Å (FOCI) and 1.548 Å (MRSDCI) and 1.591 Å (FOCI) and 1.572 Å (MRSDCI), respectively.[41] We also determine 0 K bond energies of 2.92 eV using the BHLYP functional for the $^4\Sigma^-$ ground state and a $^4\Phi$ state of 2.72 eV. These BDEs are lower than the experimental value, whereas the bond length for the $^4\Sigma^-$ state is 1.565 Å, in good agreement with the other calculations. QCISD(T)//BHLYP calculations yield a 0 K bond energy of 3.05 eV for the $^4\Sigma^-$ ground state, in very good agreement with experiment, and an excitation energy of 0.28 eV for the $^4\Phi$ state. As found by Holthausen et al.,[67] the B3LYP functional yields bond energies exceeding those for the BHLYP functional and QCISD(T) methods; however, in the present system, it appears that the B3LYP functional and QCISD(T) method perform most accurately.

We also investigate several excited states of IrH^+ at the B3LYP/HW+/6-311+G(3p) level. These states are listed in Table 3. From our calculations, we find that the $^4\Sigma^-$ ground state has a $\sigma_b^2\sigma^1\pi^4\delta^2$ valence configuration, where σ_b represents the bonding orbital and the remaining are nonbonding orbitals on the metal. Likewise, the $^4\Phi$ and $^4\Pi$ states have $\sigma_b^2\sigma^1\pi^3\delta^3$ valence configurations. We cannot distinguish these two states on the basis of their orbital occupancy, but we assign the state having the lower energy as $^4\Phi$, on the basis of Hund's rules. We also identified several doublet excited states: $^2\Delta$ ($\sigma_b^2\pi^4\delta^3$), $^2\Sigma^-$ ($\sigma_b^2\sigma^1\pi^2\delta^4$), $^2\Phi/^2\Pi$ ($\sigma_b^2\sigma^1\pi^3\delta^3$), and $^2\Pi$ ($\sigma_b^2\pi^3\delta^4$). The energy of the $^2\Pi$ ($\sigma_b^2\pi^3\delta^4$) state is lower than that of the $^2\Phi/^2\Pi$ ($\sigma_b^2\sigma^1\pi^3\delta^3$) state. All these doublet states have similar bond lengths near 1.57 Å, except $^2\Sigma^-$ which has a slightly longer bond length of 1.62 Å (Table 3). A $^4\Delta$ state has a $\sigma_b^2\sigma^2\pi^2\delta^3$ valence configuration and a high excitation energy. The large excitation energies and relatively long bond lengths of the $^4\Pi$ and $^4\Delta$ states (Table 3) suggest that these states must be occupying antibonding orbitals.

H−Ir$^+$−H. To explore coarse features of the potential energy surfaces for reaction 1, we also calculated the properties of stable IrH_2^+ complexes. Our results can be compared directly with those of Balasubramanian and Dai (BD), who calculated potential energy surfaces for the interaction of several spin states of Ir^+ with H_2 at the CAS-MCSCF level.[34] These calculations use a relativistic effective core potential on Ir that retains the *n*s and (*n* − 1)d orbitals in the valence space. In all of these calculations (ours and those of BD), the symmetry was restricted to C_{2v}.

For IrH_2^+, our B3LYP/HW+/6-311+G(3p) calculations find an inserted $^3A_2$ ground state with a BDE of 1.89 eV relative to the Ir^+ (a^5F) + H_2 asymptote. We also determine bond energies (zero point energy corrected) of 1.32 and 1.67 eV using the BHLYP functional and the QCISD(T) method for the $^3A_2$ ground state, again below the B3LYP value. BD also find a $^3A_2$ ground state with BDEs of 0.74 and 1.30 eV relative to the Ir^+ (^5D) + H_2 asymptote at the CASSCF and MRSDCI levels of theory. The main difference between the calculations of BD and those conducted here appears to be primarily a difference in the asymptotic limit. This is further confirmed by comparing the excitation energies for the various quintet and triplet states of IrH_2^+ given in Table 4. For instance, the MRSDCI excitation energies for all seven states differ from those calculated here by a mean absolute deviation of 0.23 ± 0.16 eV (the mean absolute deviations for the CASSCF values is 0.11 ± 0.10 eV). The geometries (bond lengths and angles) in the present calculations are comparable to those of BD except for the $^1A_1$ state. The bond lengths agree nicely between the present calculations and the MRSDCI and CASSCF results of BD, with mean absolute deviations of 0.011 ± 0.005 Å (MRSDCI) and 0.021 ± 0.005 Å (CASSCF) for all eight states. The bond angles also agree well except for the $^1A_1$ state with mean absolute deviations of 3.2 ± 1.9° and 1.2 ± 0.9° for the MRSDCI and CASSCF results, respectively. As discussed by BD,[34] spin−orbit effects are very significant for IrH_2^+ and the energy separations are sensitive to the inclusion of spin−orbit coupling.

Using MRCI calculations, Perry determined a $D_e(Ir^+-H_2)$ value of 1.79 eV for the $^3A_2$ ground state. After correcting for zero point energies of 0.34 eV for IrH_2^+ ($^3A_2$) and 0.27 eV for H_2, this gives a 0 K BDE of 1.72 eV for the $^3A_2$ ground state, which is comparable to our QCISD(T) and B3LYP results.[72] For the quintet states, Perry identified those states with small HIrH bond angles and long IrH bond lengths, which is different with the results from BD's calculation, who focused on states with large bond angles and short bond lengths. In our calculations, we also identified states having both kinds of structures (Table 4). Those with small bond angles and long bond lengths agree well with Perry's calculations. The mean absolute deviation between the results of Perry and our calculations are 0.07 ± 0.04 eV (excitation energies for all six excited states), 0.063 ± 0.065 Å (bond lengths for all seven states), and 2.1 ± 2.9° (bond angles for all seven states).

The complete surfaces for the various IrH_2^+ states as a function of bond angle are shown in Figure 4. These were obtained from relaxed potential energy surface scan calculations starting at the optimized geometry of each state. The character of these surfaces is generally comparable to those found by BD. For the quintet surfaces, which show saddle points attributable to avoided crossings, the detailed positions of the saddle points do vary somewhat between our calculations and those of BD.

Because the symmetry in all of the calculations was restricted to C_{2v}, these potential energy surfaces examine the evolution of $Ir^+ + H_2$ to the IrH_2^+ species as a function of the H−Ir−H angle but cannot proceed onto the $IrH^+ + H$ dissociation asymptote. However, we can anticipate that these products can be formed from the IrH_2^+ intermediates with no additional barriers. The $^4\Sigma^-$ and $^4\Phi$ states of IrH^+ can interact with H (^2S) to form both low-spin triplet and high-spin quintet states of IrH_2^+. Formation of the high-spin state would be largely repulsive because no covalent bond formation is involved, but formation of the low-spin triplet states involves covalent coupling of a nonbonding IrH^+ electron with H, such that the potential energy surface is attractive. Therefore, there should be no barriers in the exit channel of reaction 1 and its isotopologues. To verify this, we performed relaxed potential energy surface scans at the B3LYP level starting with the ground

TABLE 4: Theoretical Geometries, Energies, and Vibrational Frequencies for IrH_2^+

	this work[a]				literature[b]			literature[c]		
state	r_e(Ir−H) (Å)	∠HIrH (deg)	E_{rel}[d] (eV)	frequency (cm^{-1})	r_e(Ir−H) (Å)	∠HIrH (deg)	E_{rel}[d] (eV)	r_e(Ir−H) (Å)	∠HIrH (deg)	E_{rel}[d] (eV)
$^3A_2$	1.555	71.3	0.000	771, 2338, 2359	1.551	70.2	0.00	1.55	71.4	0.000
					(1.573)	(69.8)	(0.00)			
$^3B_1$	1.561	98.7	0.101	834, 2316, 2348	1.552	92.4	0.04	1.55	94.7	0.160
					(1.582)	(96.9)	(0.14)			
$^3A_1$	1.567	59.1	0.257	594, 2302, 2307	1.554	53.6	0.19	1.57	51.1	0.247
					(1.582)	(57.3)	(0.29)			
$^3B_2$	1.577	84.8	0.488	774, 2259, 2288	1.566	82.0	0.55			
					(1.604)	(82.3)	(0.57)			
$^1A_1$	1.542	92.3	1.054	602, 2410, 2419	1.538	59.0	0.66			
					(1.570)	(60.4)	(0.73)			
$^5B_2$	2.393	18.3	1.672	46, 358, 4125				2.42	18.1	1.630
	1.872	120.6	5.439	542, 1278, 4013						
$^5B_1$	2.524	17.3	1.727	193, 400, 4191	1.651	141.2	2.00	2.40	18.2	1.630
	1.666	143.0	2.322	873, 2032, 2289	(1.684)	(142.9)	(2.24)			
$^5A_2$	2.855	15.1	1.817	180, 250, 4275	1.635	145.0	2.00	2.99	14.4	1.722
	1.653	147.8	2.394	891, 1825, 2031	(1.678)	(148.1)	(2.24)			
$^5A_1$	2.852	15.1	1.818	190, 249, 4273	1.652	142.5	2.03	2.99	14.4	1.722
	1.668	144.7	2.337	890, 1881, 2022	(1.685)	(144.4)	(2.27)			

[a] Calculations using B3LYP/HW+/6-311+G(3p). [b] MRSDCI (CASSCF) values from Dai and Balasubramanian.[34] [c] MRCI values from Perry thesis.[72] [d] Energies relative to the ground state including zero point energies.

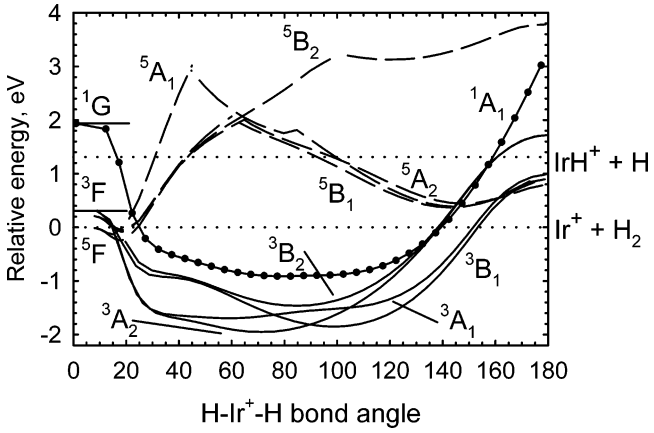

Figure 4. B3LYP/HW+/6-311+G(3p) calculations of the potential energy surfaces for the interaction of Ir^+ with H_2 in C_{2v} symmetry as a function of the H−Ir^+−H bond angle in degrees. The dotted lines indicate the experimental energy zero, corresponding to the Ir^+ (^5F) ground state, and the experimental energy of the IrH^+ + H products at 1.35 eV.

state IrH_2^+ ($^3A_2$) species and systematically lengthening one of the Ir−H bonds. These surfaces lead directly to IrH^+ ($^4\Sigma^-$) + H (^2S) with no barriers in excess of the endothermicity.

Discussion

For the three group 9 metal ions Co^+, Rh^+, and Ir^+, the BDEs are 1.98 ± 0.06,[8] 1.67 ± 0.04,[13] and 3.12 ± 0.06 eV, respectively. The stronger BDE for the iridium system can be explained by the following factors. (1) The ground state of Ir^+ is $5d^76s^1$, such that it can form a covalent bond between H(1s) and Ir^+(6s) without any promotion energy. For Co^+ and Rh^+, the ground states are $3d^8$ and $4d^8$, respectively, such that they need promotion to $3d^74s^1$ and $4d^75s^1$ (mixtures of 50% ^5F and 50% ^3F) to form covalent M^+(s)−H(1s) bonds. For Co^+, this promotion energy is only 0.82 eV,[9] and the M^+(s)−H(1s) bond is weakened from its intrinsic value of ~2.39 ± 0.07 eV by about half this amount.[9,18] For Rh^+, the promotion energy is high (2.63 eV),[9] such that RhH^+ is formed by a covalent bond between the dσ orbital of ground state Rh^+ and H (1s), where the promotion energy is much smaller, 0.29 eV,[9,13,19] but the M^+(dσ)−H(1s) bond is weaker. (2) Ir^+ can form a stronger bond by utilizing a sd hybridized orbital rather than either the pure s or pure d orbitals. This is a result of the similar size of the s and d orbitals (the 6s orbital is 1.65 times the size of the 5d orbitals),[72] an effect of the lanthanide contraction, which makes the 6s orbitals of third-row metals tighter than the 4s and 5s orbitals in the first-row and second-row congeners. Thus, the 4s orbital of Co^+ is 2.58 times the size of the 3d orbitals, and Rh^+ is intermediate with a ratio of 1.97:1 for 5s/4d.[72] These factors determine that IrH^+ has the strongest BDE, whereas Rh^+ has the weakest BDE.

To further understand these differences, we need to consider the reaction mechanisms revealed by the studies with HD. Previous work on the first-row transition metal cations indicates that the product branching ratio in the reaction of M^+ with HD is very sensitive to the reaction mechanism[10,13,14,16,17,59] and is governed by three "rules". (1) If M^+ has an electron configuration with empty 4s and 3dσ orbitals, such as for a $3d^n$ configuration where $n < 5$, the reaction is efficient and may proceed by an insertion mechanism. These processes are characterized by product branching ratios in the HD system, σ (MH^+ + D)/σ (MD^+ + H), that are near unity (or $\sigma_{MH^+}/\sigma_{total}$ values near 0.5), consistent with statistical behavior of a long-lived intermediate. (2) If either the 4s or 3dσ orbital is occupied and the M^+ state is low spin, such as for $3d^n$ ($n > 5$) or low-spin coupled $3d^{n-1}4s^1$ configurations, the reaction occurs efficiently via a direct mechanism. These processes are characterized by a product branching ratio in the HD system that favors MH^+ by a factor of 2−4 (or $\sigma_{MH^+}/\sigma_{total}$ ratios between 0.66 and 0.8), consistent with arguments concerning the conservation of angular momentum.[58,69,73−75] (3) If either the 4s or 3dσ orbital is occupied and the M^+ state is high spin (the highest spin it can possibly have), such as a high-spin coupled $3d^{n-1}4s^1$ configuration, the reaction is inefficient and tends to react impulsively. These processes are characterized by a product branching ratio in the HD system that favors MD^+ + H by a large factor (small values of the $\sigma_{MH^+}/\sigma_{total}$ ratio) and exhibit shifts in the thresholds for the H_2 and D_2 systems versus the HD system. Note that these rules are only appropriate for the diabatic reaction behavior, that is, cases where the electron configuration of the metal ions remains essentially static throughout the course of the reaction.

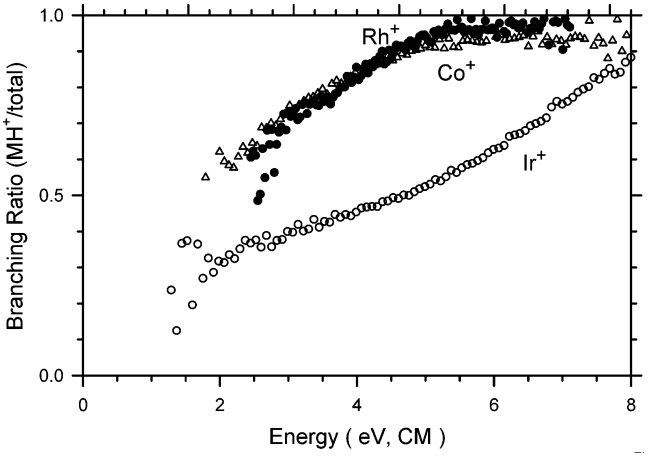

Figure 5. Product branching fractions ($\sigma_{MH^+}/\sigma_{total}$) for reactions of Co^+ (open triangles), Rh^+ (closed circles), and Ir^+ (open circles) with HD as a function of kinetic energy in the center-of-mass frame.

For the early-row congeners of group 9, the ground states of Co^+ and Rh^+ have $3d^8$ and $4d^8$ electron configurations, respectively. Thus, both of these ions should react with dihydrogen in a direct process according to "rule 2".[8,13] This expectation is verified from Figure 5; the Co^+ and Rh^+ react to form about twice as much MH^+ as MD^+ near threshold (close to 2.50 eV for Co^+ and 2.85 eV for Rh^+).

For Ir^+, according to the diabatic reactivity rules, Ir^+ (^5F, $5d^76s^1$) should react diabatically with dihydrogen according to "rule 3", that is, via an impulsive mechanism. Such a prediction is inconsistent with the experimental cross sections (Figure 3). However, in agreement with this prediction, the calculated potential energy surfaces indicate that the Ir^+ (a^5F) ground state forms a largely ion-induced dipole complex (small H−Ir−H bond angles) (Figure 4). As the bond angle increases in an attempt to insert into the H_2 bond, the energy increases. Therefore, the experimental behavior observed here at threshold is inconsistent with reaction along any of the quintet surfaces. Rather, Ir^+ behaves more like category 1, which involves a statistical intermediate. This behavior can be explained as long as this reaction system does not maintain the quintet spin when it goes along the potential energy surface. As seen from the calculated potential energy surface, there are several triplet surfaces evolving from Ir^+ (^3F, $5d^8$) configurations. These triplet states lead to strongly bound IrH_2^+ intermediates that can dissociate to the ground state $IrH^+ + H$ without barriers in excess of the product asymptote once the energy available for the reaction is sufficiently high. Therefore, reaction of $Ir^+ + H_2$ must occur by coupling the quintet and triplet surfaces (Figure 4).

For the three group 9 metal ions Co^+, Rh^+, and Ir^+, the maximum cross sections for the three metal ions reacting with dihydrogen are about 1.8, 2.8, and 2.2 ($\times 10^{-16}$ cm^2), respectively,[8,13] Oddly, the maximum cross section of RhH^+ is bigger than that of IrH^+ even though the Rh^+ reaction has the largest endothermicity. The reduced absolute reactivity of Ir^+ (^5F) may be a consequence of the coupling efficiency between the quintet and triplet surfaces. If this coupling is not completely efficient, then the observed reactivity could be reduced. On the basis of the modeling of the observed absolute cross sections (comparison of σ_0 values), such coupling can be estimated to be 30−40% efficient in the case of Ir^+. This is comparable to the 70% efficiency for dehydrogenation of CH_4 by Ir^+, as measured by Irikura and Beauchamp.[22]

Conclusions

Ground state Ir^+ ions form a strong bond with H atoms compared with the first-row and second-row transition metal systems. Analysis of the kinetic energy dependence of the reaction cross sections provides the BDE of Ir^+−H, 3.12 ± 0.06 eV. Our experimental results are in reasonable agreement with ab initio calculations performed here and in the literature. The bond dissociation energy of the IrH^+ ground state is found to be significantly larger than that for either the first- or second-row transition metal hydride cations CoH^+ and RhH^+. This difference is a consequence of lanthanide contraction and relativistic effects, which alter the relative size of the valence s and d orbitals and make 6s−5dσ hybridization more effective.

The branching ratios observed in the reactions with HD show that the ground state of Ir^+ reacts with dihydrogen largely via an insertion mechanism. This contrasts with expectations for the high-spin ground states of the metal ions that are based on diabatic reactivity rules.[17,75] In the Ir^+ system, calculations also provide a detailed potential energy surface for this reaction. This potential energy surface shows that the Ir^+ (^3F) state inserts into H_2 spontaneously, whereas there is a large barrier for Ir^+ (^5F) to insert into H_2. At threshold, reactions of Ir^+ with H_2, D_2, and HD require spin changes from quintet states to triplet states along the lowest energy path available, which apparently involves extensive spin−orbit coupling.

Acknowledgment. This research is supported by the National Science Foundation, grant CHE-0135517.

References and Notes

(1) Janowicz, A. H.; Bergman, R. G. *J. Am. Chem. Soc.* **1982**, *104*, 352. Hoyano, J. K.; Graham, W. A. G. *J. Am. Chem. Soc.* **1982**, *104*, 3723. Hoyano, J. K.; McMaster, A. D.; Graham, W. A. G. *J. Am. Chem. Soc.* **1983**, *105*, 7190. Buchanan, J. M.; Stryker, J. M.; Bergman, R. G. *J. Am. Chem. Soc.* **1986**, *108*, 1537. Foo, T.; Bergman, R. G. *Organometallics* **1992**, *11*, 1801. Foo, T. Bergman, R. G. *Organometallics* **1992**, *11*, 1811.

(2) Armentrout, P. B.; Beauchamp, J. L. *Chem. Phys.* **1980**, *50*, 37.

(3) Armentrout, P. B.; Beauchamp, J. L. *J. Am. Chem. Soc.* **1981**, *103*, 784.

(4) Armentrout, P. B.; Halle, L. F.; Beauchamp, J. L. *J. Am. Chem. Soc.* **1981**, *103*, 962.

(5) Armentrout, P. B.; Halle, L. F.; Beauchamp, J. L. *J. Am. Chem. Soc.* **1981**, *103*, 6501.

(6) Halle, L. F.; Klein, F. S.; Beauchamp, J. L. *J. Am. Chem. Soc.* **1984**, *106*, 2543.

(7) Tolbert, M. A.; Beauchamp, J. L. *J. Am. Chem. Soc.* **1984**, *106*, 8117.

(8) Elkind, J. L.; Armentrout, P. B. *J. Phys. Chem.* **1986**, *90*, 6576.

(9) Elkind, J. L.; Armentrout, P. B. *Inorg. Chem.* **1986**, *25*, 1078.

(10) Elkind, J. L.; Armentrout, P. B. *J. Phys. Chem.* **1987**, *91*, 2037.

(11) Mandich, M. L.; Halle, L. F.; Beauchamp, J. L. *J. Am. Chem. Soc.* **1984**, *106*, 4403.

(12) Elkind, J. L.; Sunderlin, L. S.; Armentrout, P. B. *J. Phys. Chem.* **1989**, *93*, 3151.

(13) Chen, Y.-M.; Elkind, J. L.; Armentrout, P. B. *J. Phys. Chem.* **1995**, *99*, 10438.

(14) Sievers, M. R.; Chen, Y.-M.; Armentrout, P. B. *J. Phys. Chem.* **1996**, *100*, 54.

(15) Schilling, J. B.; Goddard, W. A., III; Beauchamp, J. L. *J. Am. Chem. Soc.* **1986**, *108*, 582. Schilling, J. B.; Goddard, W. A., III; Beauchamp, J. L. *J. Phys. Chem.* **1987**, *91*, 5616. Schilling, J. B.; Goddard, W. A., III; Beauchamp, J. L. *J. Am. Chem. Soc.* **1987**, *109*, 5565. Schilling, J. B.; Goddard, W. A., III; Beauchamp, J. L. *J. Phys. Chem.* **1987**, *91*, 4470. Pettersson, L. G. M.; Bauschlicher, C. W., Jr.; Langhoff, S. R.; Partridge, H. *J. Chem. Phys.* **1987**, *87*, 481. Alvarado-Swaisgood, A. E.; Harrison, J. F. *J. Phys. Chem.* **1988**, *92*, 2757.

(16) Armentrout, P. B. *ACS Symp. Ser.* **1990**, *428*, 18.

(17) Armentrout, P. B. *Int. Rev. Phys. Chem.* **1990**, *9*, 115.

(18) Armentrout, P. B.; Kickel, B. L. In *Organometallic Ion Chemistry*; Freiser, B. S, Ed.; Kluwer: Dordrecht, The Netherlands, 1996; p 1.

(19) Armentrout, P. B. In *Topics in Organometallic Chemistry*; Brown, J. M., Hofmann, P., Eds.; Springer-Verlag: Berlin, 1999; Vol. 4-I, p 1.

(20) Armentrout, P. B. *Int. J. Mass Spectrom.* **2000**, *200*, 219.

(21) Irikura, K. K.; Beauchamp, J. L. *J. Am. Chem. Soc.* **1991**, *113*, 2769.
(22) Irikura, K. K.; Beauchamp, J. L. *J. Phys. Chem.* **1991**, *95*, 8344.
(23) Sunderlin, L. S.; Armentrout, P. B. *J. Am. Chem. Soc.* **1989**, *111*, 3845.
(24) Chowdhury, A. K.; Wilkins, C. L. *J. Am. Chem. Soc.* **1987**, *109*, 5336.
(25) Zhang, X.-G.; Liyanage, R.; Armentrout, P. B. *J. Am. Chem. Soc.* **2001**, *123*, 5563.
(26) Wesendrup, R.; Schröder, D.; Schwarz, H. *Angew. Chem., Int. Ed. Engl.* **1994**, *33*, 1174.
(27) Heinemann, C.; Wesendrup, R.; Schwarz, H. *Chem. Phys. Lett.* **1995**, *239*, 75.
(28) Pavlov, M.; Blomburg, M. R. A.; Siegbahn, P. E. M.; Wesendrup, R.; Heinemann, C.; Schwarz H. *J. Phys. Chem. A.* **1997**, *101*, 1567.
(29) Achatz, U.; Beyer, M.; Joos, S.; Fox, B. S.; Niedner-Schatteburg, G.; Bondybey, V. E. *J. Phys. Chem. A* **1999**, *103*, 8200.
(30) Achatz, U.; Berg, C.; Joos, S.; Fox, B. S.; Beyer, M. K.; Niedner-Schatteburg, G.; Bondybey, V. E. *Chem. Phys. Lett.* **2000**, *320*, 53.
(31) Buckner, S. W.; MacMahon, T. J.; Byrd, G. D.; Freiser, B. S. *Inorg. Chem.* **1989**, *28*, 3511.
(32) Ranasinghe, Y. A.; MacMahon, T. J.; Freiser, B. S. *J. Phys. Chem.* **1991**, *95*, 7721.
(33) Ohanessian, G.; Brusich, M. J.; Goddard, W. A., III. *J. Am. Chem. Soc.* **1990**, *112*, 7179.
(34) Balasubramanian, K.; Dai, D. *J. Chem. Phys.* **1990**, *93*, 7243.
(35) Das, K. K.; Balasubramanian, K. *J. Chem. Phys.* **1991**, *94*, 3722.
(36) Dai, D.; Balasubramanian, K. *J. Chem. Phys.* **1991**, *95*, 4284.
(37) Dai, D.; Balasubramanian, K. *Chem. Phys. Lett.* **1991**, *185*, 165.
(38) Dai, D. G.; Cheng, W.; Balasubramanian, K. *J. Chem. Phys.* **1991**, *95*, 9094.
(39) Balasubramanian, K.; Ma, Z. *J. Phys. Chem.* **1991**, *95*, 9794.
(40) Zhang, H.; Balasubramanian, K. *J. Phys. Chem.* **1992**, *96*, 6981.
(41) Dai, D. G.; Huang, A. P.; Balasubramanian, K. *J. Mol. Spectrosc.* **1992**, *154*, 345.
(42) Zhang, X.-G.; Rue, C.; Shin, S.-Y.; Armentrout, P. B. *J. Chem. Phys.* **2002**, *116*, 5574.
(43) Zhang, X.-G.; Armentrout, P. B. *J. Chem. Phys.* **2002**, *116*, 5565.
(44) Armentrout, P. B.; Li, F.-X. *J. Chem. Phys.* **2004**, *121*, 248.
(45) Loh, S. K.; Hales, D. A.; Lian, L.; Armentrout, P. B. *J. Chem. Phys.* **1989**, *90*, 5466.
(46) Schultz, R. H.; Armentrout, P. B. *Int. J. Mass Spectrom. Ion Processes* **1991**, *107*, 29.
(47) Teloy, E.; Gerlich, D. *Chem. Phys.* **1974**, *4*, 417.
(48) Gerlich, D. *Adv. Chem. Phys.* *82*, 1.
(49) Ervin, K. M.; Armentrout, P. B. *J. Chem. Phys.* **1985**, *83*, 166.
(50) Chantry, P. J. *J. Chem. Phys.* **1971**, *55*, 2746.
(51) Lifshitz, C.; Wu, R. L. C.; Tiernan, T. O.; Terwilliger, D. T. *J. Chem. Phys.* **1978**, *68*, 247.
(52) Kickel, B. L.; Armentrout, P. B. *J. Am. Chem. Soc.* **1995**, *117*, 4057.
(53) Clemmer, D. E.; Chen, Y.-M.; Khan, F. A.; Armentrout, P. B. *J. Phys. Chem.* **1994**, *98*, 6522.
(54) Haynes, C. L.; Armentrout, P. B. *Organometallics* **1994**, *13*, 3480.
(55) Kickel, B. L.; Armentrout, P. B. *J. Am. Chem. Soc.* **1995**, *117*, 764.
(56) Kleef, T. V.; Metsch, B. *Physica B & C* **1978**, *95*, 251.
(57) Chesnavich, W. J.; Bowers, M. T. *J. Phys. Chem.* **1979**, *83*, 900.
(58) Aristov, N.; Armentrout, P. B. *J. Am. Chem. Soc.* **1986**, *108*, 1806.
(59) Armentrout, P. B. In *Advances in Gas Phase Metal Ion Chemistry*; Adams, N. G., Babcock L. M., Eds.; JAI: Greenwich, CT, 1992; Vol. 1, p 83.
(60) Muntean, F.; Armentrout, P. B. *J. Chem. Phys.* **2001**, *115*, 1213.
(61) Weber, M. E.; Elkind, J. L.; Armentrout, P. B. *J. Chem. Phys.* **1986**, *84*, 1521.
(62) Huber, K. P.; Herzberg, G. *Molecular Spectra and Molecular Structure*; Van Nostrand Reinhold: New York, 1979; Vol. IV.
(63) Becke, A. D. *J. Chem. Phys.* **1993**, *98*, 5648.
(64) Lee, C.; Yang, W.; Parr, R. G. *Phys. Rev. B* **1988**, *37*, 785.
(65) Frisch, M. J.; Trucks, G. W.; Schlegel, H. B.; et al. *GAUSSIAN 98*, revision A.11; Gaussian, Inc.: Pittsburgh, PA, 1998.
(66) Hay P. J.; Wadt, W. R. *J. Chem. Phys.* **1985**, *82*, 299.
(67) Holthausen, M. C.; Heinemann, C.; Cornehl, H. H.; Koch, W.; Schwarz, H. *J. Chem. Phys.* **1995**, *102*, 4931.
(68) Holthausen, M. C.; Mohr, M.; Koch, W. *Chem. Phys. Lett.* **1995**, *240*, 245.
(69) Elkind, J. L.; Armentrout, P. B. *J. Phys. Chem.* **1985**, *89*, 5626.
(70) Armentrout, P. B. In *Gas Phase Inorganic Chemistry*; Russell, D. H., Ed.; Plenum: New York, 1989; p 1.
(71) Armentrout, P. B. In *Selective Hydrocarbon Activation: Principles and Progress*; Davies, J. A., Watson, P. L., Greenberg, A., Liebman J. F., Eds.; VCH: New York, 1990; p 467.
(72) Perry, J. K. Ph.D. Dissertation, California Institute of Technology, 1994.
(73) Sunderlin, L. S.; Aristov, N.; Armentrout, P. B. *J. Am. Chem. Soc.* **1987**, *109*, 78.
(74) Burley, J. D.; Ervin, K. M.; Armentrout, P. B. *Int. J. Mass Spectrom. Ion Processes* **1987**, *80*, 153.
(75) Armentrout, P. B. *ACS Symp. Ser.* **1992**, *502*, 194.